JOURNAL OF COMPUTATIONAL PHYSICS 99, 271–287 (1992)

# A Computer Method for Simulation of Cardiovascular Flow Fields: Validation of Approach

C. COCKERHAM VESIER AND A. P. YOGANATHAN

*Cardiovascular Fluid Mechanics Laboratory, School of Chemical Engineering, Georgia Institute of Technology, Atlanta, Georgia 30332-0100*

Received January 16, 1990; revised October 1, 1990

An existing pressure correction method to model unsteady flow with arbitrarily moving boundaries has been adapted to simulate three-dimensional blood flow in compliant vessels. This noniterative method, which is first-order time accurate, solves the three-dimensional unsteady Navier–Stokes equations with arbitrarily moving boundaries for the no slip boundary condition. It is capable of realistically modeling blood flow in the heart, since it allows the simulation of both passive tissue (e.g., heart valves) and active tissue (e.g., heart muscle fibers). The boundaries, which represent cardiovascular tissue, are displaced by the fluid motion. When they are moved, the boundaries have the ability to exert a force which opposes fluid motion. The force the boundary exerts is assumed to be proportional to strain. The results of simulating 3D pulsatile flow through a flexible tube are presented, as well as a comparison to Womersley's analytic approximate solution for axisymmetric pulsatile flow in a flexible tube. 

## INTRODUCTION

For the past two decades, computational fluid dynamics has been a useful research tool in the study of cardiovascular fluid mechanics. The value of a validated, versatile computational model, capable of simulating a wide variety of fluid flow geometries, is well known. Such a model would greatly reduce the expense of gathering experimental data by aiding the experimentalist in the interpretation of measurements and the planning of future experiments. It would also permit the gathering of data that would have been very difficult or impossible to obtain by another method.

Most previous computational models simulated two-dimensional flow in a rigid body. Several have simulated flow through heart valve-like geometry using a body-conforming grid for different flow regimes. The following groups have developed models to simulate steady laminar flow in a heart valve: Greenfield and Kolff [1], Greenfield *et al.* [2], Au and Greenfield [3, 4], Underwood and Mueller [5, 6], Bercovier *et al.* [7], Engleman *et al.* [8], and Idelsohn *et al.* [9]. With the exception of Idelsohn *et al.* which simulated flow up to a Reynolds number of 2000, all of the steady laminar flow studies were for relatively low Reynolds numbers. Steady turbulent flow through heart valve-like geometries has been simulated by Stevenson and Yoganathan [10, 11], Stevenson *et al.* [12], and Thalassoudis and Mazumdar [13]. Unsteady laminar flow through heart valve-like geometry was done by Hung and Schuessler [14, 15] and Williams [16]. Although Hung and Schuessler did simulate moving boundaries, their rigid boundaries moved according to some predetermined time course.

Recent computer research in cardiovascular fluid dynamics has taken advantage of technological advances in computer hardware. This research has primarily been directed at understanding three-dimensional biofluid flow in a rigid body, such as, flow in a curved tube [17–23], flow in the cardiac chambers, and flow in a bifurcated tube. Steady flow in a rigid carotid bifurcation has been simulated by Kleinstruer *et al.* [24] and Rindt *et al.* [25]. Simulations of unsteady flow in rigid cardiac chambers has been used for artificial heart research [26]. They assumed the heart to have rigid walls which could move according to some predefined time course.

While these simulations offered valuable insight into the particular type of fluid flow they simulated, they were unable to account for the effect of flexible boundaries. Peskin did account for the effect of flexible boundaries in his simulation of unsteady two-dimensional flow in the left heart [27–29]. Peskin's 2D algorithm is a versatile research tool because of its unique ability to deal with flexible boundaries. In subsequent work, Peskin's approach was altered to allow 3D simulations [30, 31]. It is this algorithm and its validation by comparison to the approximate analytic solution of Womersley flow that is presented here.

## METHODOLOGY

### *Model Requirements*

Ideally, we would like to model the interaction of blood flow in the cardiac chambers with the cardiac tissue. Car-



0021-9991/92 $3.00

diovascular flow can be characterized as three-dimensional unsteady flow in a compliant vessel. The cardiovascular tissue that composes the flow boundaries in the heart is either passive or active (contractile). Passive tissue, such as heart valve leaflets, exerts a force on the fluid only when resisting displacement. Active tissue, or heart muscles, is capable of exerting a time-varying force that is not a function of the flow field. The computer model should ideally be capable of modeling a three-dimensional, unsteady flow field and the flow field's interaction with both passive and active tissue.

*Overview of Algorithm*

In the early seventies, Peskin developed an immersed boundary method that satisfied all of the model's requirements except one; it was two-dimensional [27]. His model used Chorin's pressure correction algorithm to solve the two-dimensional Navier–Stokes equations for flow in the left ventricle. The heart walls, which behaved as a muscle, and mitral valve were modeled as a set of neutrally-buoyant springs that were immersed in the fluid. Contraction of the heart walls generated the force required to drive the fluid flow. The heart walls and mitral valve also exerted a force (which was a function of strain) on the fluid. At the start of each time step, the force of the heart walls and mitral valve on the fluid was computed. Based on this force, the Navier–Stokes equations were solved for the velocity field. At the end of the time step, the velocity and displacement of the heart structures were computed using the end-time-step velocity field.

To simulate a three-dimensional unsteady flow field and its interaction with flexible boundaries, the 2D algorithm was extended to 3D [30, 31]. The 3D algorithm is based on the same assumptions used in the 2D model. However, before the 3D algorithm can confidently be used to model a complex flow field, it is necessary to validate its accuracy. This is accomplished by simulating 3D pulsatile flow in a flexible tube and comparing the results to Womersley's approximate analytic solution for axially symmetric pulsatile flow in a flexible tube. The remainder of the paper deals with this validation study.

*Boundary Algorithm*

The tube wall was represented as a set of points that were free to move in response to the fluid field. Since the boundaries are not rigid, fixed structures, a system of equations must be developed and solved to predict the boundary position as a function of time. These equations must also couple the boundary and fluid together. As in Peskin's, the boundary can be described as follows:

— It is represented as a set of discrete points, on a fluid grid.

— Its points do not necessarily lie on the grid nodes.

— It is neutrally buoyant.

— It moves at the same velocity as the surrounding fluid (no slip boundary condition).

The boundary is capable of generating a force field that acts on the fluid. For the flexible tube model, a skeleton of stationary points which do not move in response to fluid motion are distributed on the fluid grid in the shape of a tube according to the following algorithm:

$$X_{i,j,1} = (Rh)\cos\frac{2\pi}{N_r}j + 32.5\,h \tag{1}$$

$$X_{i,j,2} = (Rh)\sin\frac{2\pi}{N_r}j + 32.5\,h \tag{2}$$

$$X_{i,j,3} = (0.4\,h)i, \tag{3}$$

where

$0 \leqslant i \leqslant 159$,

$1 \leqslant j \leqslant N_r$,

$N_r = 2\pi R/0.4$,

$20 \leqslant R \leqslant 24$,

$h$ = grid width = 1/64 cm.

The above algorithm is for a grid with 64 points in each direction; the tube's axial direction is along the $z$ axis and its centerline intersects with the center of the $x$-$y$ planes.

Tethered to each stationary point is one "free-moving" point. The initial position of the free-moving points is the same as its corresponding stationary point. The free-moving points move at the same velocity as the surrounding fluid. When a point is displaced from its original position by the fluid, a tension, $T_{i,j,l}$ results between the stationary point and its associated free-moving point in the $l$-direction according to the following:

$$T_{i,j,l} = E(X^*_{i,j,l} - X_{i,j,l}), \tag{4}$$

where

$E$ is the proportionality constant between strain and the resulting tension and has the units of dynes/cm$^2$,

$X^*_{i,j,l}$ is the position of stationary point, and

$X_{i,j,l}$ is the position of free moving point.

The proportionality constant $E$ is a function the tube wall thickness, tube radius, the Young's modulus of the tube, and Poisson's ratio for the tube. Since we wished to compare the simulation results to Womersley's approximate analytic solution, it was important that the analytic solution describe the same tube properties. Equation (4) was

assumed equivalent to the expression Womersley utilized if the same tension resulted from equivalent wall strain.

In the expression Womersley utilized to describe the relationship between tension and strain, there is a term known as Poisson's ratio (defined in Appendix A). This term, which does not appear in Eq. (4), describes the contribution of radial strain to longitudinal tension, as well as the contribution of longitudinal strain to radial tension. Since Eq. (4) does not include Poisson's ratio, it would appear that this equation describes a material for which Poisson's ratio is zero. Because the strain used in this model was calculated as a function of the flow field, the boundary exhibits a Poisson's ratio characteristic of an incompressible fluid, or 0.5 (versus approximately 0.4 of blood vessels). Therefore, the simulations do include the effect of a Poisson's ratio of 0.5 on the stress vector.

With the method used for the simulations presented here, the boundary displacement due to the fluid field is calculated by approximating the boundary velocity, assuming no slip between the tube wall and the fluid. Based on the displacement distance, one can estimate the force of the boundary on the fluid. The force field is discrete and is only known at the boundary point locations. To use this force in the pressure correction algorithm, one must calculate an equivalent force field known at the fluid grid nodes. The method used to calculate the boundary displacement and its resulting force field at the fluid grid nodes is based on Peskin's approach [30].

*Fluid Algorithm*

Once the fluid force field at the grid nodes is known, then a new velocity and pressure field is calculated by solving the Navier–Stokes equations in accordance with the immersed boundary method [30]. The portion of this method which solves the Navier–Stokes equations is based on a pressure correction algorithm [33].

To drive the fluid in the tube, a time varying sinusoidal axial volumetric flow rate was specified. To maintain the specified flow rate, a set of additional steps were added to the immersed boundary algorithm prior to the interpolation of the fluid velocity field to the boundary points. The first step was to calculate the volumetric flow rate over all planes, for some constant $z$, from the previous time step according to Eq. (5),

$$Q^{n-1} = \frac{h^2}{N} \sum_{I,J,K} U^{n-1}{}_{I,J,K,3}. \tag{5}$$

Then the velocity field $W^n{}_{I,J,K,L}$ which would have to be added to the velocity at the previous time step in order to achieve a specified axial volumetric flow rate was computed according to the following algorithm:

$$q^n = {}^{Q(t)}_{\text{ideal}} - Q^{n-1} \tag{6}$$

$$W^n{}_{I,J,K,3} = 0, \text{ if } |(I-32.5), (J-32.5)| > R \quad \text{(outside tube)} \tag{7}$$

$$W^n{}_{I,J,K,3} = q^n\beta, \text{ if } |(I-32.5), (J-32.5)| \leqslant R \quad \text{(inside tube)} \tag{8}$$

$$W^n{}_{I,J,K,1} = W^n{}_{I,J,K,2} = 0, \tag{9}$$

where

$\beta = 1/h^2/(\text{number of grid points inside the tube})$

${}^{Q(t)}_{\text{ideal}}$ is the desired volumetric flow.

Finally, the velocity field $W^n{}_{I,J,K}$ was added to the previous time step velocity field to compute the fractional step velocity field $U^{n,-1}{}_{I,J,K,L}$ (Eq. (10)). It should be noted that Eq. (10) is equivalent to the application of a body force equal to $\rho W/dt$:

$$U^{n,-1}{}_{I,J,K,L} = U^{n-1}{}_{I,J,K,L} + W^n{}_{I,J,K,L}. \tag{10}$$

Because of the additional fracional time step, the first fractional step in solving the Navier–Stokes equation is changed to Eq. (11) from the form utilized in Peskin's approach [30],

$$U^{n,0}{}_{I,J,K,L} = U^{n,-1}{}_{I,J,K,L} + \frac{dt}{\rho} F_{I,J,K,L}. \tag{11}$$

In the pressure correction method the final fractional step involves forcing the velocity field to have zero divergence by the addition of a velocity field which will force zero divergence [30]. The computation of this velocity field $U^{n,4}{}_{I,J,K,L}$ involves solution of Poisson's equation, with a fast Fourier transform [30]. Solution of Poisson's equation with this method does contain some inherent error. One factor which contributes to the error is the fact that Poisson's equation is solved for a cylindrical problem (flow in a tube) in the Cartesian coordinate system. Since the errors are small, they are only noticeable if the magnitude of that velocity field is close to zero, which occurs during some phases of pulsatile flow. Because we were interested in simulating pulsatile flow, minimizing these errors was desirable. To accomplish this, the velocity field $W^n{}_{I,J,K,3}$ is modified according to tangential position by the following algorithm. First, the grid points which are located inside the tube, at some constant $z$, are divided into 10 sets of 2.4 mesh width width thickness (for a tube radius of 24 mesh widths) according to the following definition:

$$\text{Points} \in \text{Set } M \text{ if } \frac{R}{10}(M-1) \leqslant |(I-32.5), (J-32.5)| < \frac{R}{10} M. \tag{12a}$$

The mean of the velocity field $U^{n,4}{}_{I,J,K,3}$ for each of the 10 sets, at some constant $z$, was computed, or

$$\langle U^{n,4}\rangle_{M,K}=\frac{1}{N_M}\sum_{\substack{\text{grid points}\\ \in \text{set } M}} U^{n,4}{}_{I,J,K,3}, \qquad (12b)$$

where $N_M$ = number of points in set $M$.

Once the mean velocity was known, the fluid velocity field $W^n{}_{I,J,K,3}$ was modified for grid points in set $M$ as:

$$W^n{}_{I,J,K,3}=W^n{}_{I,J,K,3}+\langle U^{n,4}\rangle_{M,K}-U^{n,4}{}_{I,J,K,3}. \qquad (12c)$$

It should be noted that this correction factor should be unnecessary when the fluid is driven by wall contraction, since driving the fluid by wall contraction is self-correcting for this type of error. Also, since this procedure involves radial averaging, the effective resolution of the computation was reduced. Finally, this approach did, to some small extent, enforce radial symmetry; but since the magnitude of the correction was too small in comparison to the axial velocity, the authors do not feel that this procedure had any significant effect on the radial symmetry of the pulsatile flow field. This is substantiated by the axial symmetry of the steady flow field which was not corrected in this manner.

*Selection of Model Parameters*

The parameters in the Navier–Stokes equations were selected based on physiologic norms, since the goal was to simulate physiologic flow. The parameters that were common to all of the Womersley and Poiseuille flows simulated are shown in Table I. Three Womersley numbers were simulated: 13.2, 10, and 8. The Womersley parameter, which is defined in Appendix A, is a dimensionless number that indicates the relative importance of inertial effects to viscous effects for pulsatile flow; the smaller the Womersley number, the more important the viscous effects. The highest number simulated is characteristic of the human ascending aorta; the lowest is characteristic of the human abdominal aorta. Only two parameters, the frequency and time step size, were varied to simulate different Womersley numbers. The time step size was fixed so that there would be 64 time steps in each cycle.

**TABLE I**

Womersley Flow Operating Conditions

| Parameter | Current value | Limit (if any) |
|---|---|---|
| Reynolds No. | 50 to 140 | $8\alpha^2/(3\pi)$ |
| Womersley No. | 8 to 13.2 | — |
| Tube radius | 24 grid widths | — |
| Grid width | 0.015625 cm | — |
| Time step | 2.6 to 7.2 ms | — |
| Young's modulus | 5,000,000 dynes/cm$^2$ | Same |
| Kinematic viscosity | 0.03 cm/s$^2$ | — |
| Axial pressure gradient | 270 to 2300 dynes/cm$^3$ | $ph/dt^2$ |
| Tube wall thickness | 10% of tube radius | — |

*Approach to Validating the 3D Algorithm*

The 3D model was validated by comparison to Womersley's analytic solution for 2D pulsatile flow in a flexible tube as follows:

— Two different types of flow were simulated with the model: steady or Poiseuille flow at a Reynolds number of 20, and Womersley flow. The Womersley simulations were performed for three different Womersley parameters, 13.2, 10, and 8, at peak Reynolds numbers ranging between 140 and 50.

— The four Womersley constants that described the flow field for each test cases were computed. Womersley derived his solution using complex numbers, while the simulation was done with only real numbers. So although the complex flow field was calculated, only its real part was compared to the simulations. Details on how the complex Womersley constants were computed are available in Appendix B.

— The analytical and numerical predictions for the axial fluid and boundary motion were compared by graphs. It was not possible to constrast the model's predictions for the radial boundary and fluid motion to Womersley's predictions because of model limitations (see Results section, *Oscillatory Flow*, below).

— A 3D animated movie was made of the model's predictions for the axial flow field.

— The relative magnitude of the disagreement between the numerical and analytical solutions for the axial velocity field was computed. The error was not computed for the axial boundary displacement because it would have been meaningless. Womersley's solution for a flexible tube is known to over-predict the magnitude of axial wall motion in comparison to experimental observations [33].

## RESULTS

The computer simulation of fluid flow through a flexible tube marches forward in time and requires approximately 1.5 cpu minutes per time step. At each time step, the model estimates the fluid velocity field resulting from the driving force and tube configuration known at the start of each time step. The tube is assumed to be immersed in the fluid and is treated as a specialized area of the fluid. This specialized area is capable of exerting a force.

For the analytical solutions to Womersley and Poiseuille flow, air is assumed to surround the tube, which implies that the velocity of the fluid very close to the external surface is zero, even if the tube wall is moving. Therefore, the fluid

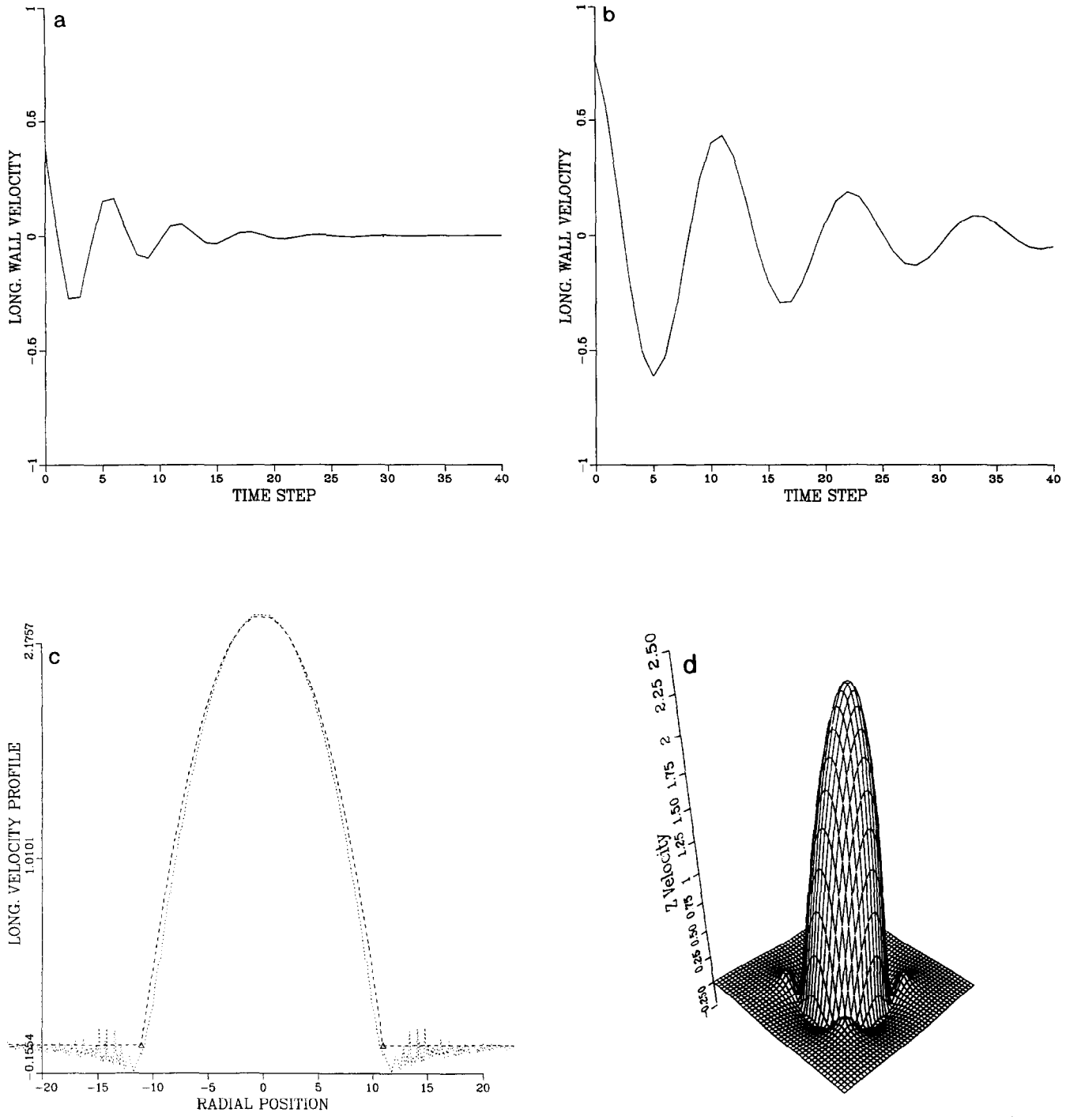


**FIG. 1.** (a) and (b). The approach to equilibrium (zero velocity) of the longitudinal wall velocity, at a Reynolds number of 20 (a); Reynolds number of 64 (b). (c) and (d). Poiseuille flow for a Reynolds number of 20. The dotted line is the model's prediction; the dashed line is the analytic solution.

velocity gradient across the tube wall approaches a discontinuity, which is not observed in the simulations. The simulated velocity field is smoothed because the tube is assumed to be surrounded by the same fluid that flows through it. The gradient at the wall should approach reality under two conditions. First, there must be sufficient grid points in the near wall region to simulate the velocity gradient. Second, the model must be allowed enough time steps to asymptotically approach the true velocity field resulting from a tube wall configuration and driving force. When simulating steady flow in a flexible tube, the longitudinal wall velocity will initially be very high, approximately one-half that of the mean fluid velocity. The longitudinal wall velocity should approach zero as time goes to infinity, so this velocity should indicate if the method is converging to the true velocity field and how fast it is converging. In Fig. 1a and b, one can see that the computed flow field does converge to the true velocity field as time goes to infinity and that the higher the Reynolds number, the slower the convergence. With Poiseuille flow the driving force is constant for all time steps and adequate time was permitted to find the gradient. With Womersley flow the driving force changes at every time step, so it is likely that there is some error in the near wall velocity field, especially for the relatively high Womersley numbers simulated.

*Steady Flow*

The steady flow case, which simulates Poiseuille flow in a tube that was 40 mesh widths in diameter at a Reynolds number of 20, was done as a first step in validating the algorithm, since it is the simplest case. Steady state was reached after 40 time steps or 200 ms when the maximum change in the axial velocity field between time steps was less that 0.01 %. Figure 1c shows the smooth parabolic shape of the steady-state axial velocity profile. If this model were perfect, there would have been no radial flow. However, radial flow did occur because of radial boundary motion and the inaccuracy of the algorithm used to solve Poisson's equation (Poisson's equation is solved when calculating the pressure field necessary for zero velocity divergence). This inaccuracy is directly related to the number of grid points; the more points, the more accurate the solution. Nevertheless, the inaccuracy in this algorithm is not noticeable in the axial velocity profiles because the axial velocity is large compared to the error.

Figure 1d, the axial velocity profile in 3D, establishes that the internal flow field is axially symmetric, but there are small deviations in the external axial flow field as one moves around the tube at constant radial position. These "velocity bumps" in the flow field are the result of not correcting the velocity field which was added to the end time step velocity field to drive the fluid. As previously reviewed in the Methodology section, these tangential variations at constant radial position occur when simulating axially symmetric flow in a Cartesian coordinate system.

*Oscillatory Flow*

With increasing Womersley number, one would expect the axial velocity profile to change from a parabolic shape to a blunter, or plug flow shape. This is because as the Womersley number increases (inertial effects become more important), frequency increases, and the amount of time available to develop a parabolic profile decreases, so the profile becomes blunter. Figure 2 shows the axial velocity profile at 45°-intervals in the phase angle for a sinusoidal flow cycle, for three Womersley numbers 13.2, 10, and 8. As expected, the axial velocity profile became blunter with increasing Womersley numbers. Also in Fig. 2, one can see that the fluid in the center of the pipe possesses more momentum than that at the edges, since it is moving faster. Because of the momentum associated with the fluid in the center of the pipe, the centerline axial velocity profile lags behind the driving force. This lag results in the dip in the

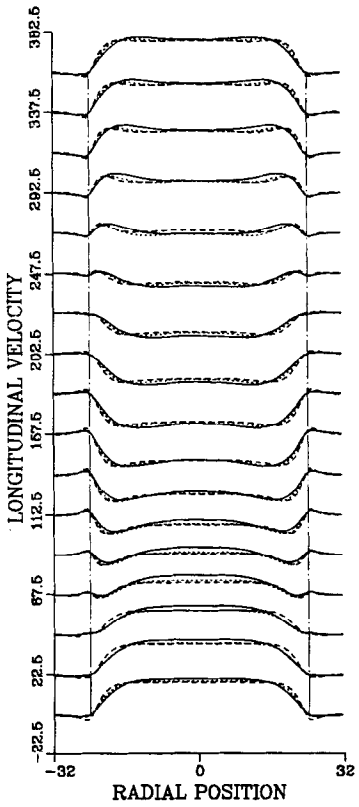


**FIG. 2.** Axial velocity profile for Womersley flow at different phase angles. The solid line corresponds to Womersley parameter of 8 and Reynolds number of 50; the dotted line is 10 and a Reynolds number of 80; and the dashed line is 13.2 and a Reynolds number of 140. The broken lines are tube walls.

centerline axial velocity profile that is characteristic of pulsatile flow.

The velocity field for any phase angle is a function of two items, the system parameters, such as frequency, pressure gradient and Young's Modulus, and the fluid field of the previous phase. If the program was allowed to run long enough so that the effect of the second item was the same for every cycle (zero transient effects), then the velocity profiles for phases 180° apart would be mirror images of each other (see Fig. 2). They are not because only one and a half cycles were simulated to reduce computer time. While some transient effects are present for the entire simulation, they are most noticeable in data collected early in the run, or between 0 and 180°. In Womersley flow, transient effects are assumed to be negligible.

One simulation at a Womersley number of 10 was conducted to test the convergence to the periodic steady state. If the flow converges, the flow at one phase should be the mirror image of the flow at that phase plus 180°. Figure 3a establishes that the flow did converge; in fact the difference between the forward and reverse velocity profiles is so small (less than 0.1% difference) that the two flow fields appear identical. An animated movie of this simulation was also made. Selected frames of the movie are shown in Fig. 3b which illustrates the radial symmetry of these 3D axial velocity profiles, both inside and outside the tube; i.e., the "velocity bumps" that were seen in Fig. 1b, Poiseuille flow in 3D, are not apparent here. The fluid field irregularities were eliminated by correcting the velocity field added to the end time step field to move the fluid for tangential variations in the pressure field.

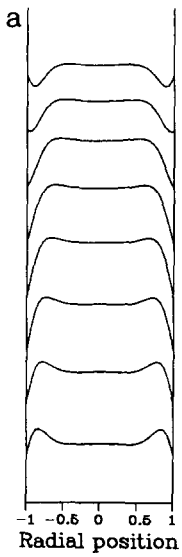


**FIG. 3.** (a) Comparison of axial velocity profile for a Womersley number of 10 of phases separated by 180°. The solid line represents forward flow; the dashed line represents the backward flow field. Note for comparison purposes the backward flow was multiplied by a $-1$; also the differences between the forward and reverse flow are too small to be percieved.

The time course of the axial boundary position was also computed. The direction of the axial boundary motion corresponded to the flow direction for a given phase. The boundary displacement decreased with increasing Womersley number. This was expected, since increasing Womersley number decreases the time associated with one complete cycle. Reducing the cycle time decreases the net force applied to the boundary between 270 and 90° (forward flow), and between 90 and 270° (backward flow), which decreases the maximum absolute boundary displacement.

Radial fluid and boundary motion are caused by two different effects, the pressure difference across the flexible tube wall and satisfaction of the continuity equation. Since pressure is a dependent variable, one cannot specify a pressure field with this method. In Womersley's approximate analytic solution, the radial pressure gradient inside the tube is assumed to be zero, and there is a time-varying pressure difference across the tube wall. In the computer model, it was impossible to specify a radial pressure difference across the tube wall and zero radial pressure gradient within the tube, so we decided not to specify a pressure gradient across the tube wall. Our decision was justified by the fact that Womersley's analytic solution is limited to very small radial boundary displacements, i.e., a very small pressure difference across the tube wall. The actual difference between the bulk internal fluid pressure and bulk external pressure was $10^{-6}$ dynes/cm$^2$. The gradient at the wall was less than single precision accuracy.

With pulsatile flow in a flexible tube, axial velocity varies down the length of the tube because of a finite pulse wave speed (see Eq. (13)). Since axial velocity is a function of axial position, the continuity equation demands radial flow. With these simulations, the pulse wave speed approached infinity, because the volumetric flow rate was not a function of axial position. An infinite pulse wave speed implies that axial velocity is not a function of axial position; therefore there would be zero radial motion caused by satisfying the continuity equation. With a very large wave speed and a very small pressure gradient across the tube wall one would anticipate very little or no radial boundary or fluid motion. That is what the model predicted. The radial boundary motion, which is a function of the weighted average of the radial fluid velocity close to the tube wall, was zero. The radial fluid velocity, which was close to zero, reflects the inherent error associated with this approach. To permit radial velocity and boundary motion the wave speed must be finite. Because of the boundary conditions this algorithm utilized, the pulse wavelength is limited to values less than the grid's axial dimension. The grid's axial dimension is of the same order of magnitude as the tube radius. Since Womersley derivation assumes that the pulse wavelength is

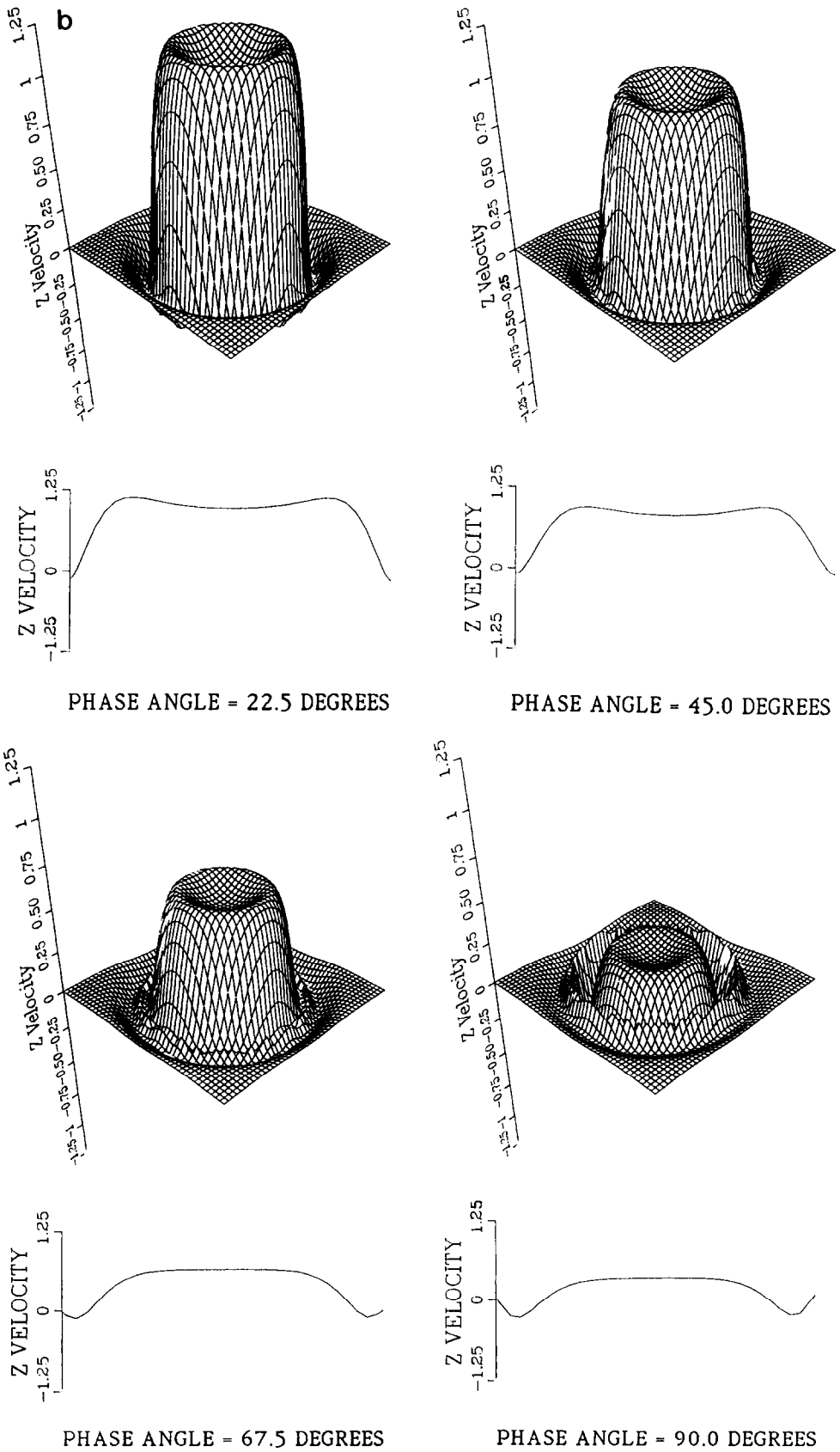


**FIG. 3.** (b) Axial velocity profile for a Womersley number of 10, and a Reynolds number of 80 at 45° phase angles.

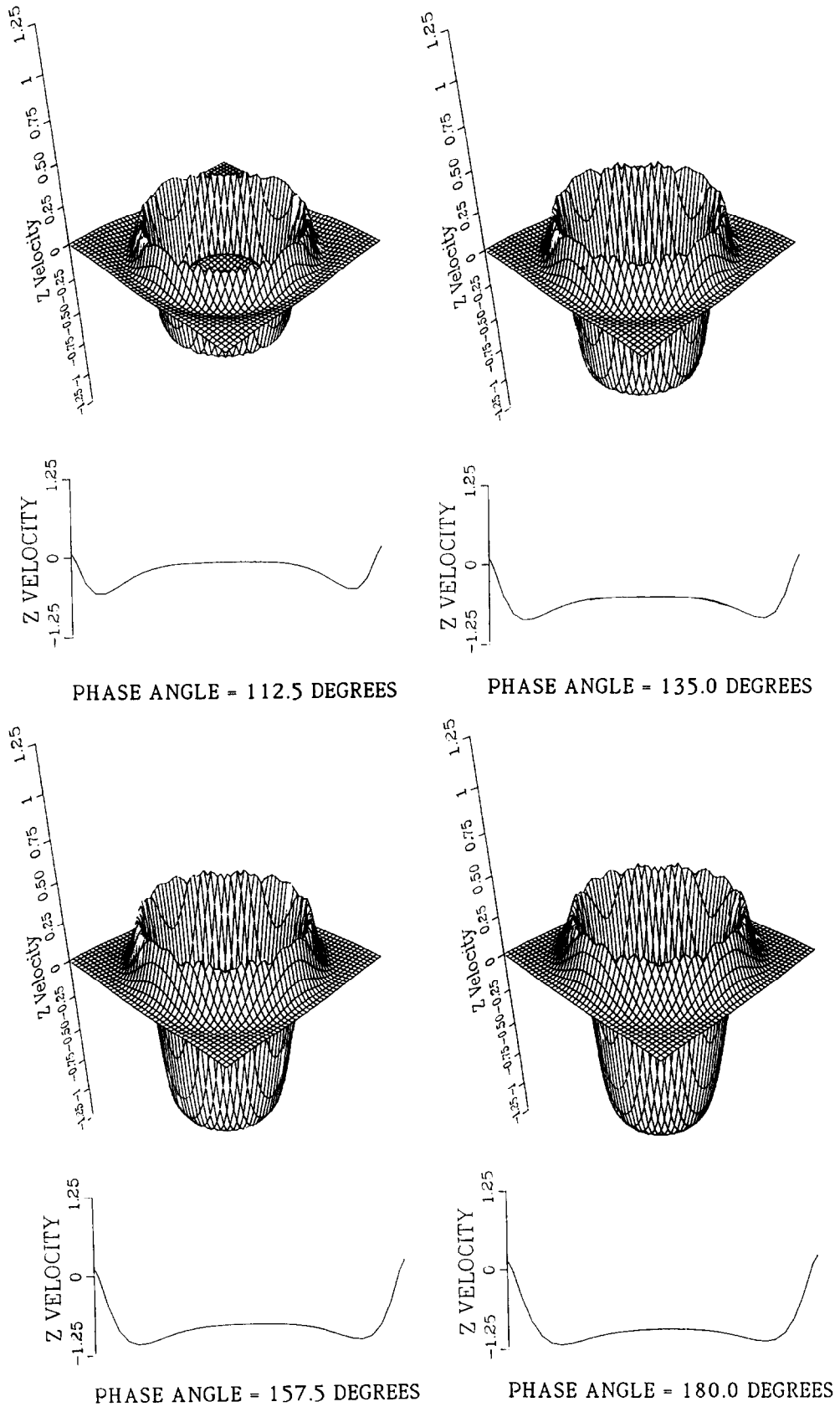


**FIGURE 3b**—*Continued*

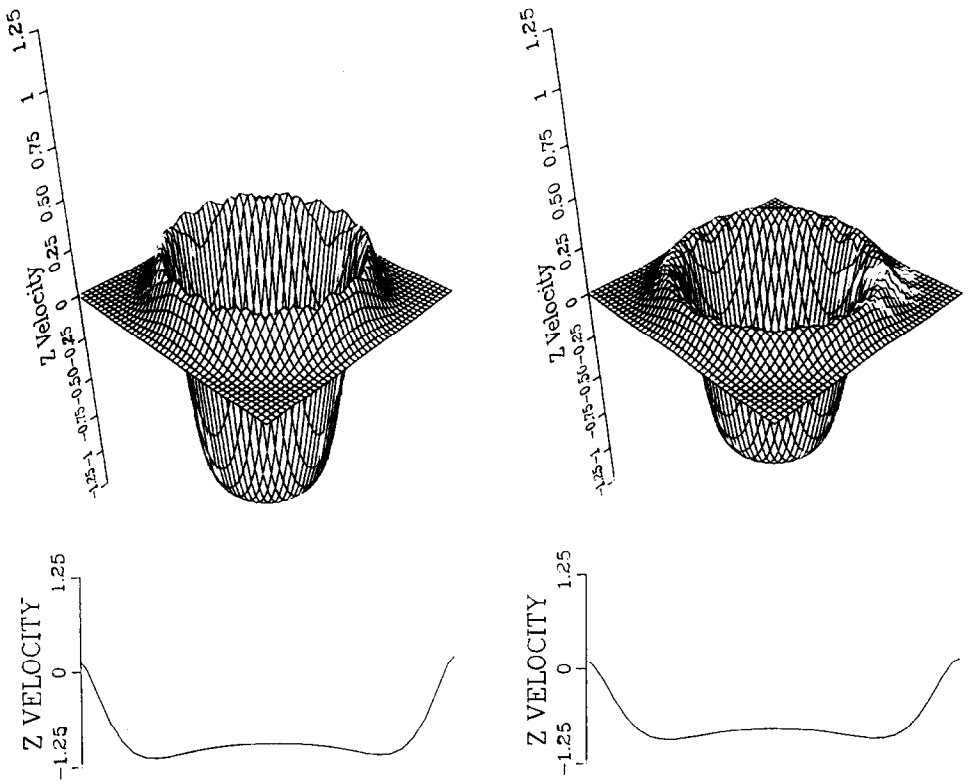


PHASE ANGLE = 202.5 DEGREES PHASE ANGLE = 225.0 DEGREES

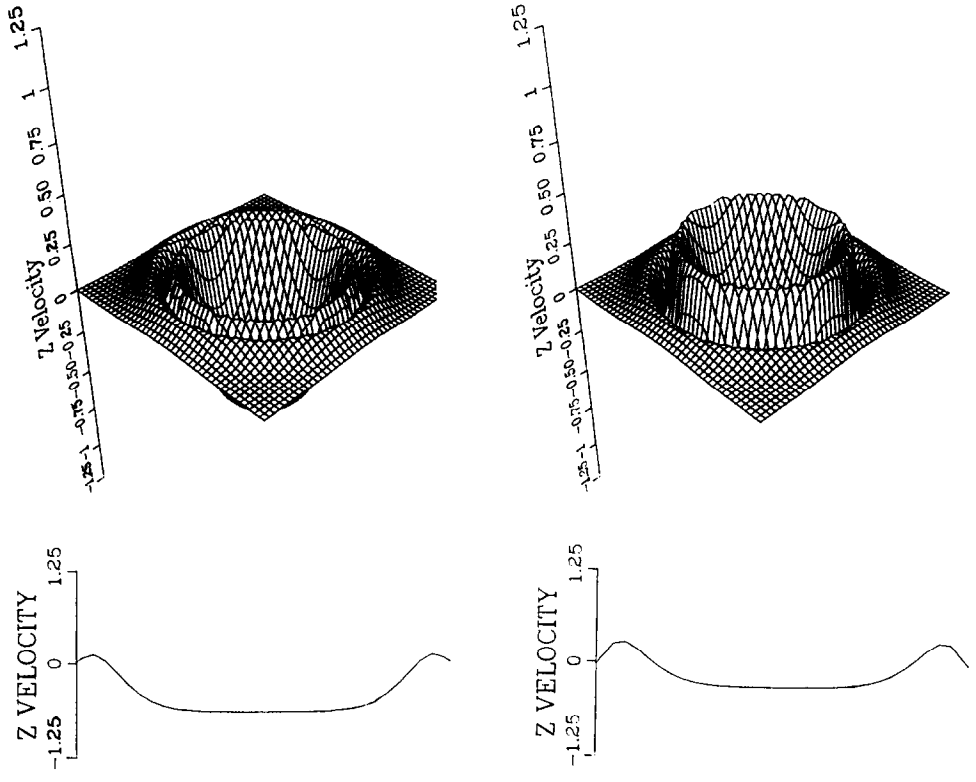


PHASE ANGLE = 247.5 DEGREES PHASE ANGLE = 270.0 DEGREES

**FIGURE 3b**—*Continued*

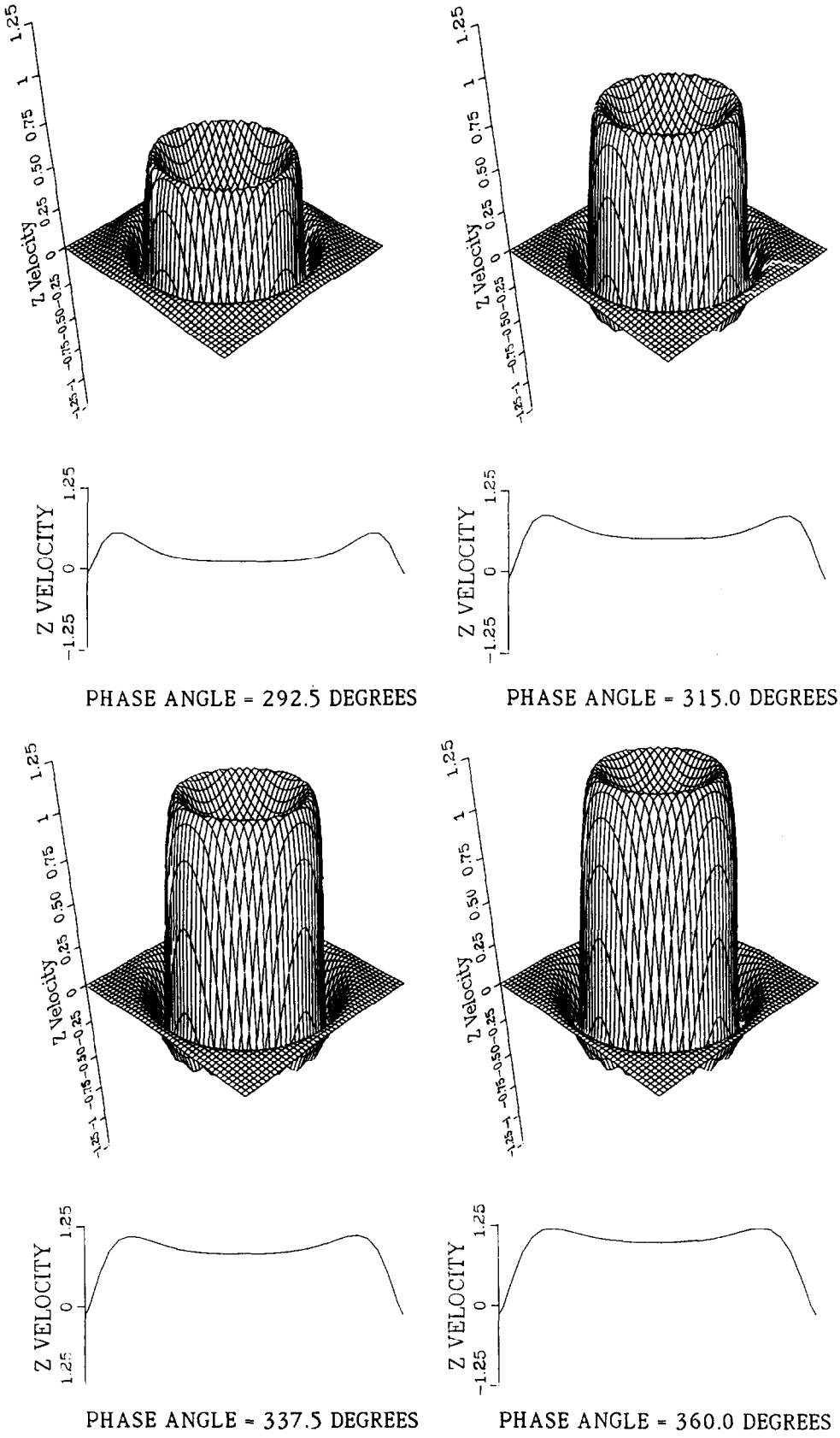


**FIGURE 3b**—*Continued*

much greater than the tube radius, simulations that would allow comparison of the radial velocity and boundary motion to Womersley's approximate analytic solution are not possible.

## DISCUSSION

Overall, the method was found to accurately predict pulsatile flow in flexible tube. Since the approach is independent of body geometry, it is reasonable to assume that it is capable of simulating pulsatile or steady flow through a large variety of flexible geometries. The main limitation of the method is that it is limited to low Reynolds numbers (less than 500 for the geometry used in this study), by the Courant–Friedrichs–Lewy stability condition, which requires the maximum grid velocity not to exceed that required to travel one grid width in one time step. Although the authors are aware that this method has in the past been limited to a local Reynolds number of less than two, based on grid mesh width, some of these test cases exceeded that limit. The authors can only speculate that the local Reynolds number limit must be dependent on the flow field simulated. Since a large number of physiologic flow fields can be characterized by a low Reynolds number, the limitation does not pose a problem for simulating physiologic flow. In fact, the method is capable of simulating unsteady, 3D, low Reynolds number flows through a wide variety of compliant bodies.

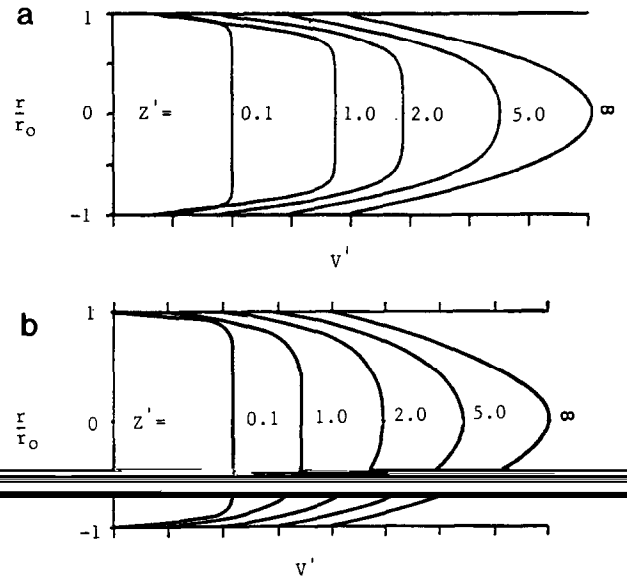


**FIG. 4.** (a) and (b) Comparison of approach to equilibrium of axial velocity, $v'$, for equivalent nondimensional axial position, $z'$. View $A$ is computational flow; view $B$ is analytically determined developing flow in the entrance region [34]. In both views the axial velocity and position are nondimensional (velocity by mean velocity and axial position by tube radius). Note the axial position is normalized by Reynolds number, so as to be Reynolds number independent.

*Steady Flow*

Although the model's prediction is virtually identical to the analytical solution, there are small discrepancies in the near wall region. The relative maximum error at this location is 12% (overall the model's predictions are within 2% of the true solution). The error in the vicinity of the wall is the result of two factors. First, the model will not allow a discontinuity in the velocity gradient across the tube wall. Second, there are insuffucient grid points within the tube (tube diameter = 40 mesh widths) to accurately simulate the velocity gradient. An additional case study was conducted in which the number of points within the tube was reduced by one half. Reduction in the number of grid points within the tube increased the error by 350%.

Because this method marches forward in time, it is important to know if the time the computed flow field required to converge to the expected solution was dominated by the algorithm or the physics of the problem. Insight into the factors that governed the convergence of the steady flow field can be obtained by comparing the computed flow to flow in the entrance region of a pipe. Entrance region flow has been studied extensively by Langhaar [34]. The

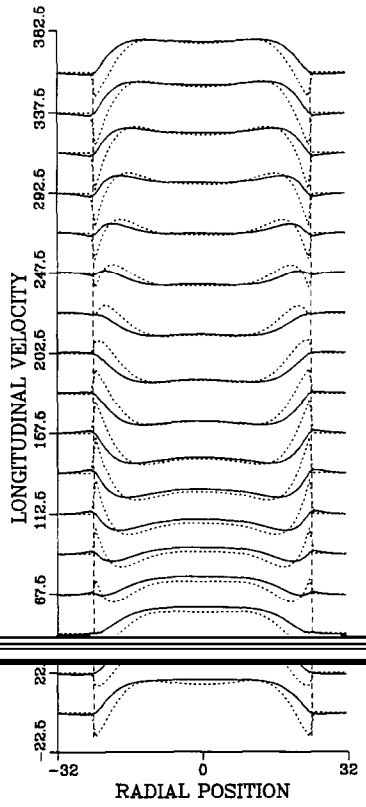


**FIG. 5.** Axial velocity profile for a Womersley number of 8 and a Reynolds number of 50 in a flexible tube, at different phase angles. The solid line is the model's prediction; the dotted line is the analytic solution; and the dashed lines are the tube walls.

development of the computed flow profile as a function of time can be viewed in a Lagrangian sense as the entrance flow down a tube; the axial position of the simulated flow field would correspond to the mean velocity of the fluid multiplied by the elapsed time. Figure 4 compares the developing simulated axial velocity profile, which has been nondimensionalized by mean velocity, to that analytically determined by Langhaar at equivalent dimensionless axial locations. Axial position was nondimensionalized and scaled so as to be independent of Reynolds number according to the following formula:

$$\text{Non-dimensional axial position} = \frac{200Z}{N_{re}R},$$

where

$R$ is the radius of the tube,

$Z$ is the axial position in centimenter,

$N_{re}$ is the Reynolds number, and

for the computational tube, $Z$ or the axial position was defined as the mean velocity times the elapsed time.

One can deduce from these two plots that the time required for the numerical flow field to converge to the steady state solution was dominated by the physics of the problem, not the numerical approach.

*Oscillatory Flow*

The model's predictions were compared against Womersley's analytic solution for pulsatile flow in a tube (see Fig. 5–7). The model accurately predicted the axial flow field in the center of the pipe. The predicted axial velocity was within 3% of that calculated with Womersley's solution for the region within 67% of the tube radius from the centerline. However, there are large discrepancies between the analytical solution and the model's predictions for the flow field adjacent to the wall. These discrepancies are primarily the result of differences in the axial wall motion; Womersley's solution, which over-predicts the axial wall motion in comparison to experimental observation [33], predicted a tube motion five to six times larger than that observed with the computational tube (see Fig. 8). That the computational tube motion is less than that predicted by Womersley is not surprising, since the computational tube

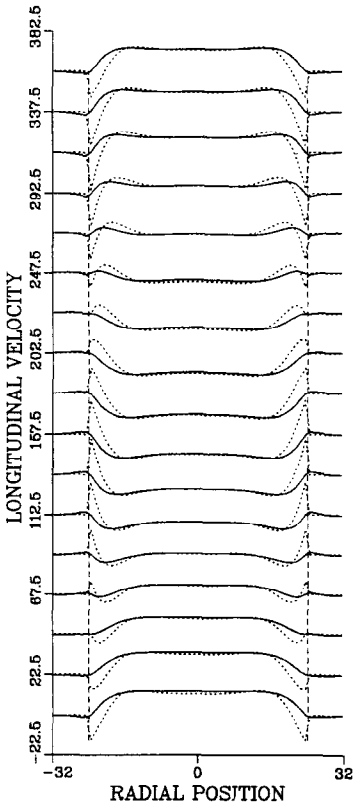


FIG. 6. Axial velocity profile for a Womersley number of 10 and a Reynolds number of 80 in a flexible tube at different phase angles. The solid line is the model's prediction; the dotted line is the analytic solution, and the dashed lines are the tube walls.

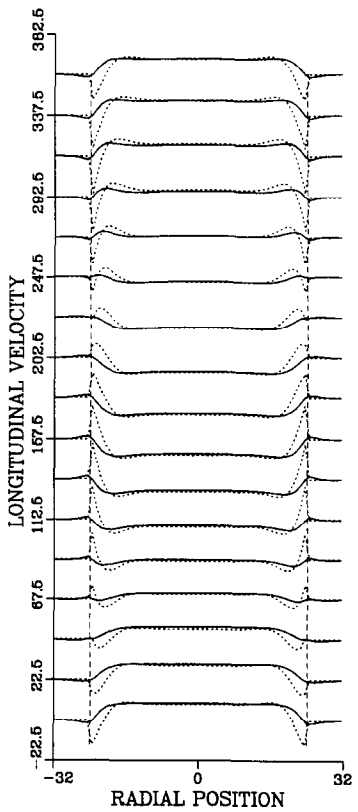


FIG. 7. Axial velocity profile for a Womersley number of 13.2 and a Reynolds number of 140 in a flexible tube at different phase angles. The solid line is the model's prediction; the dotted line is the analytic solution; and the dashed lines are the tube walls.

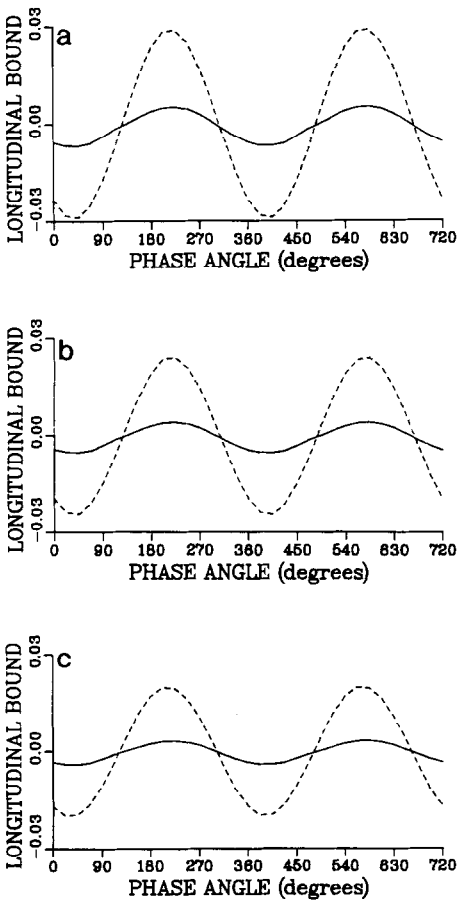


**FIG. 8.** Axial boundary motion for a Womersley number of 8 , 10, and 13.2. The solid line is the model's prediction; the dashed line is the analytic solution.

had massive fluid both inside and out, whereas Womersley's tube only had fluid within it. The mass of fluid adjacent to the inside of the tube was roughly equal to the externally adjacent mass, so the additional fluid dragged along by the computational wall was approximately twice that of the Womersley tube. From this analysis, one would expect the Womersley tube displacement magnitudes to be twice that of the computational tube, not five to six times larger. The additional dampening of the computational tube wall motion can be attributed to how computational strain was determined. As with arteries and veins which have elastic attachments to surrounding tissue, the computational tube was tethered to stationary points, so strain was determined relative to these fixed points. With Womersley's tube, strain was a funcion of the displacement of the tube wall relative to itself. It should be noted that although the model correctly predicted an axial wall displacement less than that predicted by Womersley, it is probable that the simulation under-predicted the movement because the presence of a viscous fluid outside the tube would tend to dampen any boundary motion.

If the discrepancies between the simulation results and Womersley approximate analytic solution for a flexible tube are primarily the result of overestimating of the boundary motion by Womersley's approximate analytic solution, one would expect improved agreement in the near wall region by comparing the flow field to the analytic solution for pulsatile flow in a rigid tube. Figures 9 through 11 compare the model's predictions to a rigid tube (the difference between the analytical and numerical solution is 3% within 90% of the tube radius from the centerline). As would be expected, the model predicts *more* flow reversal than the analytical solution for a rigid tube in the vicinity of the wall because the walls are not truly rigid. Since the simulations had *less* flow reversal than the analytic flexible tube solution, the model's predictions are consistent with known limitations to Womersley's approximate analytic solution.

In a flexible tube, the pulse wave speed is finite (less than 1000 cm/s); in a rigid tube it is infinite. The simulated pulse wave speed, which was calculated to be 50,000 cm/s using Eq. (19) (in Appendix B), approached infinity. This is much larger than the analytically estimated wave speed of 500 cm/s because the flow was driven by a specified axial volumetric flow rate which was a function of time only.

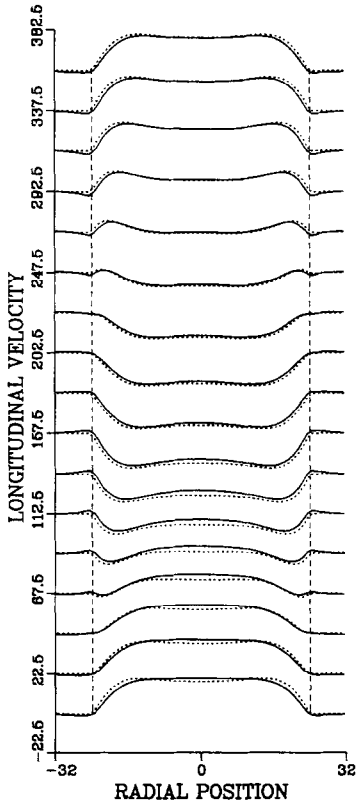


**FIG. 9.** Axial velocity profile for a Womersley number of 8 and a Reynolds number of 40 in a flexible tube compared against analytic solution for pulsatile flow in a rigid tube at different phase angles. The solid line is the model's prediction; the dotted line is the analytic solution; the dashed lines are the tube walls.

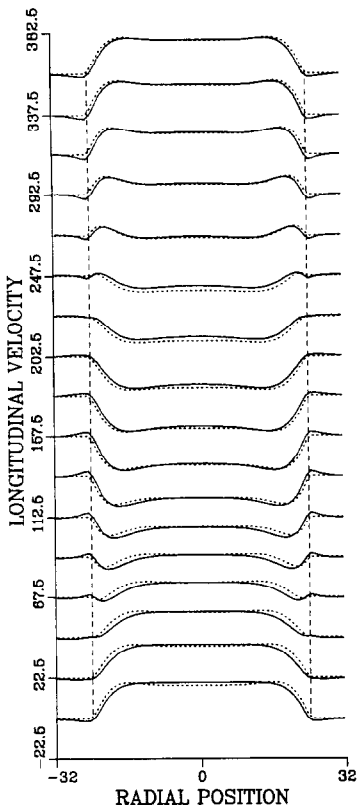


**FIG. 10.** Axial velocity profile for a Womersley number of 10 and a Reynolds number of 80 in a flexible tube compared against analytic solution for pulsatile flow in a rigid tube at different phase angles. The solid line is the model's prediction; the dotted line is the analytic solution; and the dashed lines are the tube walls.

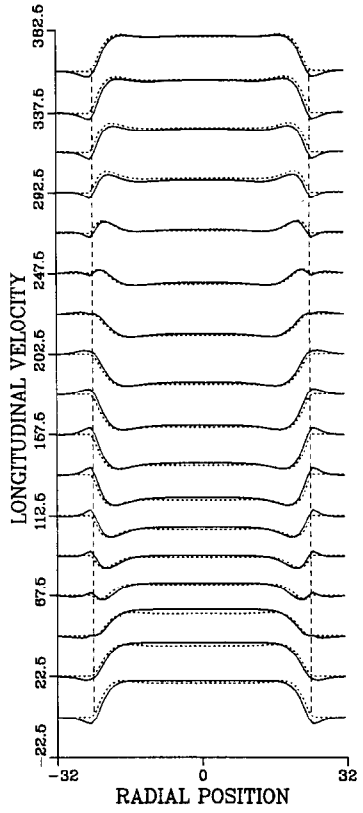


**FIG. 11.** Axial velocity profile for a Womersley number of 13.2 and a Reynolds number of 140 in a flexible tube compared against analytic solution for pulsatile flow in a rigid tube at different phase angles. The solid line is the model's prediction; the dotted line is the analytic solution; and the dashed lines are the tube walls.

Since the pulsatile simulations exhibit characteristics of flow in a rigid tube such as zero radial fluid or boundary motion, effectively infinite pulse wave speed, and axially independent velocity profile, one might ask how can the authors justify labeling these simulations as pulsatile flow in a flexible tube? To answer this question consider pulsatile flow in a flexible tube at a fixed axial location. If the pulse wavelength is very long in comparison to the tube circumference, which is true for these case studies, the tube radius can be assumed constant and the radial velocity is very small in comparison to the axial velocity. For this case, the radial fluid and boundary motion contribute very little to the axial profile at fixed axial position. The primary effect of the flexible boundary is that the fluid velocity at the wall oscillates about zero because of time-varying axial wall strain. Because strain was defined relative to a fixed set of points, the effect of a flexible wall, i.e., time varying strain, was included in the simulations. Since time-dependent axial strain is the primary ingredient which causes the characteristic axial velocity profile, we feel that these simulations model pulsatile flow in a flexible not rigid tube.

## CONCLUSIONS

Overall, the method compared well with both Womersley and Poiseuille flow. The discrepancies between the model's predictions and the approximate analytic solution were confined to the near wall flow region and the magnitude of the boundary motion. These discrepancies are primarily the result of two fundamental differences between the Womersley model and the computational model. First, the computational tube had fluid both inside and out, while Womersley's tube only had fluid in its interior. Fluid outside the tube would tend to smooth the axial gradient at the wall i.e., at a discontinuity. In addition, the massive external fluid increased the effective mass of the computational tube, which would dampen the axial wall motion. Finally, the computational tube was assumed to be tethered to stationary points, unlike Womersley's tube. These attachments, which were physiologically realistic, since arteries and veins have elastic attachments to surrounding tissue, increased the computational wall resistance to motion. As a result Womersley's tube over-predicted axial wall motion in

comparison to both the computational tube and experimental observations.

This method does not change with body geometry, so it is probable that this approach can be used to simulate pulsatile or steady flow though a large variety of flexible geometries, such as flow in tubes with a bifurcatio, flow in straight tubes, flow in curved tubes, and flow in the cardiac chambers. In the future, the method will be adapted to simulate the motion of a heart valve leaflet. For this simulation, the leaflet points will be attached to their neighbors, not to stationary points. In addition, a heart valve leaflet really is surrounded by fluid, so it is anticipated that the difficulties that occurred in simulating tube wall motion will not be encountered.

## APPENDIX A: NOMENCLATURE

*Boundary*

| | |
|---|---|
| $E$ | Proportionality constant which relates strain to tension |
| $S$ | Strain, or the distance between points $X^*$ and $X$ |
| $T_{i,j,k}$ | Tension between points $X$ and $X^*$ |
| $X$ | Free-moving points |
| $X^*$ | Stationary points |

*Fluid*

| | |
|---|---|
| $\upsilon$ | Kinematic viscosity |
| $U$ | Fluid velocity |
| $N$ | Number of points on the grid in each direction ($N = 64$) |
| $N_M$ | Number of points in set $M$ |
| $dt$ | Time step size |
| $h$ | Mesh or grid width |
| $Q^n$ | Volumetric flow for time step $n$ |
| $Q(t)_{\text{ideal}}$ | Desired volumetric flow for time equal to $n\,dt$ |
| $W^n$ | Velocity field required to drive fluid |
| $U^{n,-1}$ | First fractional step velocity field resulting from imposing a volumetric flow rate |
| $U^{n,0}$ | Second fractional step velocity field resulting from boundary forces acting on fluid |
| $U^{n,4}$ | Last fractional step velocity field calculated to force zero divergence |
| $\langle U^{n,4} \rangle_{M,K}$ | Mean of final fractional step velocity field for points in set $M$, at some axial location $K$. |

*Womersley*

| | |
|---|---|
| $A_1, C_1, D_1, E_1$ | Womersley constants |
| $W$ | Axial velocity |
| $V$ | Radial velocity |
| $\xi$ | Radial boundary motion |
| $\zeta$ | Axial boundary motion |
| $w$ | Circular frequency |
| $c$ | Pulse wave speed |
| $\alpha$ | Womersley parameter; $Rw/v$ |
| $\rho_0$ | Tube wall density |
| $\rho$ | Fluid density |
| $y$ | Dimensionless radial position, $r/R$ |
| $k$ | Ratio of tube wall thickness to tube radius |
| $\sigma$ | Poisson's ratio = (Young's modulus)/(2 * shear modulus) − 1 |
| $z$ | Axial position |
| $A$ | Cross-sectional area of pipe |

*Subscripts*

| | |
|---|---|
| $I, J, K$ | $x, y, z$ location of the grid point on the grid, respectively |
| $L$ | Direction of the velocity vector |
| $i, j$ | Refers to boundary points |
| $l$ | Refers to $x, y, z$ direction |
| $M$ | Refers to grid points in set $M$ |

*Superscripts*

| | |
|---|---|
| * | Free moving boundary point |
| $n$ | Time step $n$ |

## APPENDIX B

Womersley described pulsatile flow through a flexible thin-walled tube with a system of five differential equations, the continuity and momentum equations for axial and radial flow, and the equations that described the axial and radial wall displacement [33]. In his derivation, he made six assumptions.

— The fluid obeyed the no-slip boundary condition at the wall.

— All convective terms were negligible.

— The second-order differential terms in the axial direction were negligible.

— The magnitude of the radial wall displacement was small in comparison to the tube diameter.

— The flow was driven by an oscillating pressure of the form of $p = p_0 e^{iwt}$.

— Inertial terms were neglected.

With these differential equations and assumptions, he solved for the pulse wave speed, the axial and radial fluid velocity, as well as the axial and radial boundary motion (Eq. (13) through (17)):

$$c = \left( (1-\sigma^2)\frac{kB}{\rho} \Big/ (G \pm (G^2 - (1-\sigma^2)H)^{1/2}) \right)^{1/2} \quad (13)$$

$$\xi = D_1 e^{iw(t-z/c)} \quad (14)$$

$$\zeta = E_1 e^{iw(t-z/c)} \quad (15)$$

$$W = \left( C_1 \frac{J_0(\alpha i^{3/2} y)}{J_0(\alpha i^{3/2})} + \frac{A_1}{\rho c} \right) e^{iw(t-z/c)} \quad (16)$$

$$V = \frac{iwr}{2c} \left( C_1 \frac{2J_1(\alpha i^{3/2} y)}{\alpha i^{3/2} J_0(\alpha i^{3/2})} + \frac{A_1 y}{\rho_0 c} \right) e^{iw(t-z/c)}, \quad (17)$$

where

$$H = \frac{1+2k}{1-F_{10}} - 1.$$

$$G = \frac{1.25-\sigma}{1-F_{10}} + \frac{k}{2} + \sigma - 0.25$$

$$F_{10} = \frac{2J_1(\alpha i^{3/2} y)}{\alpha i^{3/2} J_0(\alpha i^{3/2})}.$$

To compare the model's predictions to that of the analytic solution, the four Womersley's constants must be estimated. Since the force to drive the fluid flow was calculated by fixing the volumetric flow rate, it was decided to calculate the Womersley's constants based on the volumetric flow rate. Equation (18) shows the relationship between the volumetric flow rate and the Womersley coefficients:

$$Q = \text{Real} \left\{ \left( C_1 \frac{2J_1(\alpha i^{3/2})}{\alpha i^{3/2} J_0(\alpha i^{3/2})} + \frac{A_1}{\rho c} \right) e^{iw(t-z/c)} \right\}. \quad (18)$$

In Eq. (18), $A_1$ and $C_1$ are imaginary numbers, so there are four unknowns and four equations are needed. Only two of the four equations can be obtained from Eq. (18) by varying the phase angle, because of linear dependence. To simplify the mathematics, peak forward flow, or a phase angle of 360°, and zero net flow, or a phase angle of 270° were selected. Two other equations were needed. It was arbitrarily decided to use the equation for centerline axial velocity for the two phases.

## ACKNOWLEDGMENTS

This research was made possible by a computer grant from Cray Research Inc. for time on the Cray YMP, located at the Pittsburgh Supercomputing Center. Fellowship support for the first author was provided by Medtronic, Inc.

## REFERENCES

1. H. Greenfield and W. Kolff, *J. Am. Med. Assoc.* **219**, 69 (1972).
2. H. Greenfield, A. Au, S. Kelsey, and W. Kolff, *Trans. Am. Soc. Artif. Intern. Organs* **20**, 673 (1974).
3. A. Au and H. S. Greenfield, *Comput. Biol. Med.* **4**, 279 (1975).
4. A. Au and H. S. Greenfield, *Comput. Biomed. Res.* **10**, 165 (1977).
5. F. Underwood and T. Mueller, *J. Biomech. Eng.* **99**, 91 (1977).
6. F. Underwood and T. Mueller, *J. Biomech. Eng.* **101**, 198 (1979).
7. M. Bercovier, M. Engelman, and J. Borman, in *Computing Methods in Applied Sciences and Engineering*, edited by R. Glowinski and J. L. Lions (North-Holland, Amsterdam, 1980), p. 571.
8. M. Engleman, S. Moskowitz, and J. Borman, *J. Thorac. Cardiovasc. Surg.* **79**, 402 (1980).
9. S. Idelsohn, L. Costa, and R. Ponso, *J. Biomech.* **18**, 97 (1985).
10. D. Stevenson and A. Yoganathan, in *AIChe Symposium Series 79*, edited by J. Tarbell (American Institute of Chemical Engineers, New York, 1983), p. 145.
11. D. Stevenson and A. Yoganathan, *J. Biomech.* **18**, 899 (1985).
12. D. Stevenson, A. Yoganathan, and F. Williams, *J. Biomech.* **18**, 909 (1985).
13. K. Thalassoudis and J. Mazumdar, *Med. Biol. Eng. Comput.* **22**, 529 (1984).
14. T. Hung and G. Schuessler, in *Advances in Bioengineering, Chemical Engineering Progress Symposium Series 67*, edited by R. Ruckles (American Institute of Chemical Engineers, New York, 1971), p. 8.
15. T. Hung and G. Schuessler, *J. Biomech.* **10**, 597 (1971).
16. F. Williams, A. Yoganathan, and C. Cockerham, submitted for publication.
17. F. Van de Vosse *et al.*, *Int. J. Numer. Meth. Fluids* **9**, 275 (1989).
18. H. Mazher, Ph. D. thesis, Georgia Institute of Technology, Atlanta, GA, 1987 (unpublished).
19. H. Mazher and D. Giddens, *AIAA J.*, in press.
20. H. Mazher and D. Giddens, in *1987 Biomechanics Symposium, ASME AMD*, edited by D. L. Butler and P. A. Torzilli (ASME, New York, 1987), Vol. 84, p. 61.
21. H. Mazher and D. Giddens, submitted for publication.
22. A. Mazher, J. Ekaterinaris, and D. Giddens, "A Computational Approach to Biomedical Fluid Dynamics," Paper BE18-D.4, The World Congress on Medical Physics and Biomedical Engineering, San Antonio, TX, August 1988.
23. A. Mazher and J. Ekaterinaris, in *Proceedings, 14th Northeast Bioengineering Conference*, edited by J. R. Lacourse (Institute of Electrical and Electronic Engineers, New York, 1988), p. 273.
24. C. Kleinstruer *et al.*, in *Proceedings, Annual International Conference of the IEEE Engineering in Medicine and Biology Society Annual Conference*, edited by G. Harris and C. Walker (Institute of Electrical and Electronic Engineers, New York, 1988), Part 2, p. 552.
25. C. Rindt *et al.*, *J. Biomech.* **20**, 499 (1989).
26. S. Rogers, P. Kutler, D. Kwak, and C. Kiris, in *Proceedings, Fourth International Conference on Supercomputing*, edited by L. Karatashev and S. Karatashev (International Supercomputing Institute Inc., St. Petersburgh, 1989), p. 1.
27. C. Peskin, *J. Comput. Phys.* **25**, 220 (1977).
28. C. Peskin, *Flow Patterns Around Heart Valves* (Lectures on Mathematical Aspects of Physiology, American Mathematical Society, 1981), p. 69.
29. C. Peskin, *Ann. Rev. Fluid Mech.* **14**, 235 (1982).
30. C. Peskin and D. M. McQueen, *J. Comput. Phys.* **81**, 372 (1989).
31. C. Peskin and D. M. McQueen, *J. Comput. Phys.* **82**, 289 (1989).
32. A. Chorin, *J. Comput. Phys.* **2**, 12 (1967).
33. J. Womersley, WADC Report TR 56-614, 1957 (unpublished).
34. H. L. Langhaar, *J. Appl. Mech.* **9-2**, A55 (1942).